

Article

A 3D Coordination Polymer Based on *Syn-Anti* Bridged $[\text{Mn}(\text{RCOO})_2]_n$ Chains Showing Spin-Canting with High Coercivity and an Ordering Temperature of 14 K

Soumen Kumar Dubey¹, Maxcimilan Patra¹, Kajal Gupta¹, Subham Bhattacharjee^{1,*}, Rajat Saha^{1,2,*} and Carlos J. Gómez-García^{2,*} 

¹ Department of Chemistry, Kazi Nazrul University, Asansol 713340, West Bengal, India

² Departamento de Química Inorgánica, Universidad de Valencia, 46100 Burjasot, Valencia, Spain

* Correspondence: sbpb2012@gmail.com (S.B.); rajat.saha@uv.es (R.S.); carlos.gomez@uv.es (C.J.G.-G.)

Abstract: A new 3D manganese(II) coordination polymer, formulated as $[\text{Mn}_3(\text{HL})_6]$ (**1**) (where H_2L = 6-hydroxypicolinic acid), has been hydrothermally synthesized and characterized by single-crystal X-ray crystallographic analysis along with other spectroscopic and magnetic techniques. Structural analysis shows that the compound crystallizes in the monoclinic $C2/c$ space group and is a non-porous 3D coordination polymer formed by three different Mn(II) centres connected by 6-hydroxypicolinic acid ligands in their *keto* form. Each Mn(II) centre shows a distorted octahedral coordination environment. Neighbouring Mn(II) centres are connected by two different *syn-anti* bridging carboxylate groups to form regular coordination chains. There are two different $[\text{Mn}_2(\text{RCOO})_2]$ units along the chain, formed by two crystallographically independent Mn centres (Mn1 and Mn2). These chains are further connected by HL^- ligands to form a 3D coordination network. Interestingly, both the hydroxy and the carboxylate groups of the ligands are deprotonated and coordinated to the metal centres, whereas the pyridyl group is protonated and uncoordinated, although it participates in strong hydrogen bonding interactions with oxygen atoms of the HL^- ligand, as shown by the Hirshfeld surface analysis. Both the absorption and emission spectra of the compound have also been measured. Variable temperature magnetic studies reveal the presence of a spin-canted antiferromagnetic behaviour with a high coercivity of 40 mT at 2 K and an ordering temperature of 14 K.

Keywords: 3D coordination polymer; manganese(II); 6-hydroxypicolinic acid; keto-enol tautomerism; *syn-anti* carboxylate; spin-canting; magnetic properties



Citation: Dubey, S.K.; Patra, M.; Gupta, K.; Bhattacharjee, S.; Saha, R.; Gómez-García, C.J. A 3D Coordination Polymer Based on *Syn-Anti* Bridged $[\text{Mn}(\text{RCOO})_2]_n$ Chains Showing Spin-Canting with High Coercivity and an Ordering Temperature of 14 K.

Magnetochemistry **2023**, *9*, 55.

<https://doi.org/10.3390/magnetochemistry9020055>

magnetochemistry9020055

Academic Editors: Walter Alberto Cañón Mancisidor, Diego Venegas Yazigi and Fabrice Pointillart

Received: 6 January 2023

Revised: 2 February 2023

Accepted: 8 February 2023

Published: 10 February 2023



Copyright: © 2023 by the authors. Licensee MDPI, Basel, Switzerland. This article is an open access article distributed under the terms and conditions of the Creative Commons Attribution (CC BY) license (<https://creativecommons.org/licenses/by/4.0/>).

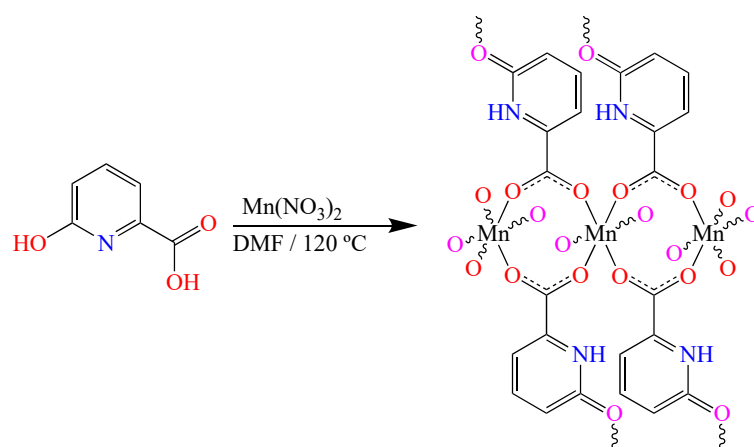
1. Introduction

The design of metal-organic coordination polymers has gained much attention for their tuneable structural features and enormous functionalities [1–5]. The search for different molecule-based magnets that show spontaneous magnetization below a critical temperature has also been an attractive field of research [6–11]. Thus, many types of magnetic coordination polymers with different topologies and dimensionalities have been developed, and their magnetic properties have been studied [12–15]. In most cases, mixed N,O-donor ligands are used to create a magnetic exchange pathway between the paramagnetic metal centres in those polymeric materials [16–19]. Albeit, it is still very difficult to control and predict the geometry and magnetic behaviour of the polymers due to the diverse coordination modes of many ligands and the sensitivity of the magnetic interactions to slight structural modifications [20–22]. Among the different strategies used to design magnetic materials, the most successful ones are: (i) the use of isolated magnetic building blocks to design extended structures [23,24], (ii) the use of radical-based bridging ligands [25–27], and (iii) the synthesis of magnetic molecules inside the cavity of metal-organic frameworks and covalent organic frameworks [28,29]. Moreover, the presence of three paramagnetic

metal centres in the basic building block of homometallic complexes and coordination polymers may induce interesting magnetic properties due to an imbalance of the overall magnetic moments [30–32].

Picolinic acids bearing hydroxy groups are very versatile ligands as their coordination behaviour is dependent on their *keto-enolic* tautomerism [33,34]. In the *keto* form, they coordinate with the carboxylate and *keto* groups, while the protonated pyridyl N atom remains uncoordinated [35]. In the *enolic* form, they can use their three different coordination sites (hydroxy, carboxylate, and pyridyl). In 6-hydroxypicolinic acid, the proximity of the hydroxy group and the basic pyridyl N atom facilitates the migration of the hydroxy proton to the pyridyl N atom, resulting in the deprotonation of the OH group and protonation of the pyridyl N atom (*keto* form). However, the coordination modes of the ligand and, therefore, the resulting nuclearities and dimensionalities are difficult to control [36]. A search in the CCDC database shows that there is a total of 29 reported structures with the ligand 6-hydroxypicolinic acid. In 16 of these structures, the ligand is totally deprotonated (L^{2-}). In nine structures, the ligand is present as the *enol* (O-H) tautomer, whereas only in four structures, it presents its *keto* (N-H) form (Table S1). In the literature, there are some examples of metal complexes with 6-OHpicH with both transition metals and lanthanoids, and most of them are monomer or discrete metal clusters [37–39]. In fact, among the 29 structures, there are three with lanthanoids (Dy^{III} , Er^{III} , and Yb^{III}), two with alkaline metals (Cs^+ and Na^+), and 24 with transition (Mn^{III} , Co^{II} , Ni^{II} , Cu^{II} , Ru^{II} , Re^{II} , Re^{III} , Re^{IV} , and Re^V) and post-transition (Zn^{II} and Cd^{II}) metal ions. Surprisingly, there is no example of any compound with this ligand and manganese(II) (Table S1). From the structural point of view, 23 of these 29 compounds are discrete complexes (there are 11 monomers, 9 dimers, and 3 trimers), and only 6 are polymers (one 1D, three 2D, and two 3D). The two only reported 3D examples are obtained with Na^+ and Cs^+ . Compound **1** is, therefore, the first 3D polymer with a transition metal and the first one with manganese(II) and 6-hydroxypicolinic acid. Furthermore, compound **1** is one of the very few compounds with this ligand in its *keto* tautomer (only 4 out of 29 to date).

Here we report the first coordination polymer obtained with the ligand 6-hydroxypicolinic acid (H_2L) and Mn^{II} : $[Mn_3(HL)_6]$ (**1**). This compound is a 3D coordination polymer formed by Mn^{II} centres connected by the *keto* form of the deprotonated 6-hydroxypyridine carboxylate ligand (Scheme 1). As the pyridyl N atom is protonated, only the deprotonated carboxylate and hydroxy groups are coordinated with the Mn^{II} atoms. There are two different Mn^{II} centres ($Mn1$ and $Mn2$) that form two different dimeric units: one contains one $Mn1$ and one $Mn2$ atom ($Mn1-Mn2$), whereas the other contains two $Mn2$ atoms ($Mn2-Mn2$). In both dimeric units, the Mn atoms are connected by *syn-anti* carboxylate groups giving rise to $[Mn_2(RCOO)_2]$ dimers, which are interconnected by carboxylate bridges to generate alternating zigzag chains of the type $[Mn(RCOO)_2]_n$. These chains are further connected by four HL^- ligands through their *keto* groups to generate a 3D coordination polymer. We also present the magnetic properties that show that compound **1** is a spin-canted antiferromagnet with an ordering temperature of ca. 14 K and a coercive field of 49 mT at 2 K. The Hirshfeld surface analysis has also been performed to understand the intramolecular interactions mainly originated by the protonated pyridyl groups.



Scheme 1. Synthetic scheme of compound **1**.

2. Materials and Methods

$\text{Mn}(\text{NO}_3)_2 \cdot 6\text{H}_2\text{O}$ and 6-hydroxypicolinic acid were purchased from Sigma Aldrich chemical company and were used as received. All other chemicals were purchased from commercial sources and used without further purification. Elemental analysis (C, H, N) was carried out using a Perkin-Elmer 240C elemental analyser. IR spectra were recorded via the ATR method using a SHIMADZU IRA 1S WL instrument within the range of $500\text{--}4000\text{ cm}^{-1}$. Absorption spectra were recorded on SHIMADZU UV 1800 instrument in solution. Emission spectra were recorded by using SHIMADZU RF 1000 instrument in solution. Powder X-ray diffraction patterns were recorded by using $\text{Cu-K}\alpha$ radiation (Bruker D8; 40 kV, 40 mA).

Synthesis of $[\text{Mn}_3(\text{HL})_6]$ (1**).** 0.2 mmol (80.8 mg) of $\text{Mn}(\text{NO}_3)_3 \cdot 6\text{H}_2\text{O}$ and 0.2 mmol (27.2 mg) of 6-hydroxypicolinic acid were dissolved in 5 mL of DMF via ultrasonication. The solution was poured into a 15 mL sealed glass vial and heated at $120\text{ }^\circ\text{C}$ for 72 h to yield rhombic-shaped colourless crystals suitable for single-crystal X-ray diffraction. The reaction mixture was allowed to cool naturally to room temperature, and crystals were isolated by filtration. Yield: 30%. Anal. Calcd. For $\text{C}_{36}\text{H}_{24}\text{Mn}_3\text{N}_6\text{O}_{18}$: C = 43.48%, H = 2.41% and N = 8.45%. Found: C = 43.50%, H = 2.40% and N = 8.45%. IR (cm^{-1}): 3400 (N-H), 1660 (C=O, keto), 1652 (ν_{asym} -COO), 1634 (C-N), 1614 (N-H), 1590 (C=O, carboxylate), 1550 (C=O, keto), 1469, 1410, 1378 (ν_{sym} -COO), 1337 (ν_{sym} -COO), 1259, 1105, and 1000. The X-ray powder diffractogram is identical to the simulated one, confirming the phase purity of compound **1** (Figure S1).

Single crystal data collection and structure refinement: Suitable single crystal of **1** was mounted on Bruker APEX II diffractometer having graphite monochromator and $\text{Cu-K}\alpha$ ($\lambda = 1.54\text{ \AA}$) radiation. Unit cell parameters were calculated by using the APEX2 program [40]. Data reduction was done by the SAINT program [40] and absorption correction was performed by using the SADABS program [40]. The structure was solved by using Patterson method through SHELXS-2018/3 [41] using WINGX software package [42] and refined by using SHELXL-2018/3 [43]. Difference Fourier synthesis and least-square refinement have pointed out the positions of the non-hydrogen atoms. The non-hydrogen atoms were refined with independent anisotropic displacement parameters. All the hydrogen atoms were placed in their calculated positions and their displacement parameters were fixed to be 1.2 times larger than the attached non-hydrogen atom. The hydrogen atoms attached to the pyridyl groups are located from the Fourier map and refined freely. Figures were drawn by PLATON [44] and ORTEP [45]. Data collection, structure refinement parameters and crystallographic data of **1** are given in Table 1.

Table 1. Crystallographic data collection and refinement parameters.

Formula	C ₃₆ H ₂₄ Mn ₃ N ₆ O ₁₈
Formula weight	993.43
Crystal system	Monoclinic
Space group	C2/c (No. 15)
a (Å)	12.3872 (13)
b (Å)	15.4999 (13)
c (Å)	20.7172 (17)
α (°)	90
β (°)	105.713 (4)
γ (°)	90
V (Å ³)	3829.1 (6)
Z	4
ρ _{calc} (g/cm ³)	1.723
μ (Mo Kα) (mm)	1.065
F(000)	2004
Crystal size (mm ³)	0.10 × 0.12 × 0.16
Temperature, T (K)	127
θ _{min-max} (deg)	2.6, 27.2
Total data	21,514
Unique data	4249
R _{int}	0.079
Observed data [I > 2.0 σ(I)]	3104
N _{ref}	4249
N _{par}	294
R	0.0479
wR ₂	0.1177
S	1.06

$$w = [(F_o^2) + (0.0287 P)^2 + 13.3720 P] \text{ where } P = (F_o^2 + 2F_c^2)/3.$$

Variable temperature magnetic measurements: Variable temperature susceptibility measurements were carried out in the temperature range 2–300 K with an applied magnetic field of 0.1 T on a polycrystalline sample with a mass of 13.598 mg using a Quantum Design MPMS-XL-5 SQUID magnetometer. The isothermal magnetization was measured at 2 K with magnetic fields in the −5 to 5 T range on the same sample. AC susceptibility measurements were performed in the temperature range of 2–18 K on the same sample with an alternating field of 0.4 mT oscillating at 10 and 110 Hz. The susceptibility data were corrected for the sample holder previously measured using the same conditions and for the diamagnetic contribution of the samples as deduced by using Pascal's constant tables [46].

Hirshfeld surface analysis: Hirshfeld surface analysis can depict and quantify the intermolecular interactions present within a crystal system. It is described from the electron distribution around a molecular entity which gives the clear visualization of the intermolecular interactions present in the crystal. 2D fingerprint plots are calculated from the HS analysis to identify and calculate the relative contributions to the total Hirshfeld surface of different intermolecular interactions. Every point on the HS is calculate by d_i (distance from the nearest nucleus internal to the surface) and d_e (distance from the nearest nucleus external to the surface).

$$d_{norm} = \frac{(d_i - r_i^{vdW})}{r_i^{vdW}} + \frac{(d_e - r_e^{vdW})}{r_e^{vdW}}$$

where r_i^{vdW} and r_e^{vdW} are the van der Waals radii of the appropriate atoms internal and external to the HS. Hirshfeld surfaces and their corresponding 2D fingerprint plots were calculated over the constituent ionic and molecular geometries using CRYSTALEXPLORER 17.5 software package [47,48]. The properties such as normalized contact distance d_{norm} , shape index, curvedness, and fragment patch were mapped over the Hirshfeld surface

and plotted with the appropriate colour scale. The 2D fingerprint plots were presented as d_e vs. d_i .

3. Results and Discussion

3.1. Synthesis

The solvothermal reaction between $\text{Mn}(\text{NO}_3)_2$ and 6-hydroxypicolinic acid (H_2L) in a 1:1 mole ratio in DMF leads to the formation of a 3D coordination polymer with the molecular formula $[\text{Mn}_3(\text{HL})_6]$ (**1**) having a metal:ligand ratio of 1:2. Within the structure, the ligand is in its *keto* form, and the pyridyl group remains protonated (Scheme 1). IR spectroscopic analysis also supports the presence of the protonated pyridyl group within the structure (Figure S2). The presence of broad peaks in the $3300\text{--}3600\text{ cm}^{-1}$ and 1614 cm^{-1} regions indicates the presence of a protonated pyridyl group within the structure [49]. This section may be divided into subheadings. It should provide a concise and precise description of the experimental results, their interpretation, as well as the experimental conclusions that can be drawn.

3.2. Structure of $[\text{Mn}_3(\text{HL})_6]$ (**1**)

Single-crystal X-ray analysis reveals that compound **1** is a 3D non-porous coordination polymer showing the $(3,6)\text{-}c\text{ rtl}$ topology [50] that crystallizes in the monoclinic space group $C2/c$. The asymmetric unit contains two independent Mn atoms: Mn1 (with half occupancy) and Mn2 (with full occupancy), and three HL^- ligands with a protonated pyridyl group and deprotonated hydroxy and carboxylate groups. The ligand-to-metal ratio is, therefore, 2:1, resulting in the formula $[\text{Mn}_3(\text{HL})_6]$ for compound **1**. Both Mn centres show distorted octahedral geometry (Figure 1). The coordination environments of both Mn atoms are identical: the equatorial positions around are occupied by three carboxylate oxygen atoms (O1, O1*, and O8* for Mn1 and O4, O5, and O7 for Mn2) and one hydroxy oxygen atom (O9* for Mn1 and O6 for Mn2) from four different HL^- ligands. The axial positions are occupied by one carboxylate (O8 for Mn1 and O5* for Mn2) and one hydroxy oxygen atom (O9 for Mn1 and O6* for Mn2) from two different HL^- ligands. So, both Mn atoms are surrounded by six different HL^- ligands. All the Mn–O bond distances fall in the range of $2.126(3)\text{--}2.224(3)\text{ \AA}$, and all *cisoid* and *transoid* angles fall in the range of $79.25(10)\text{--}102.60(10)^\circ$ and $165.00(10)\text{--}176.70(10)^\circ$, respectively (Table S2).

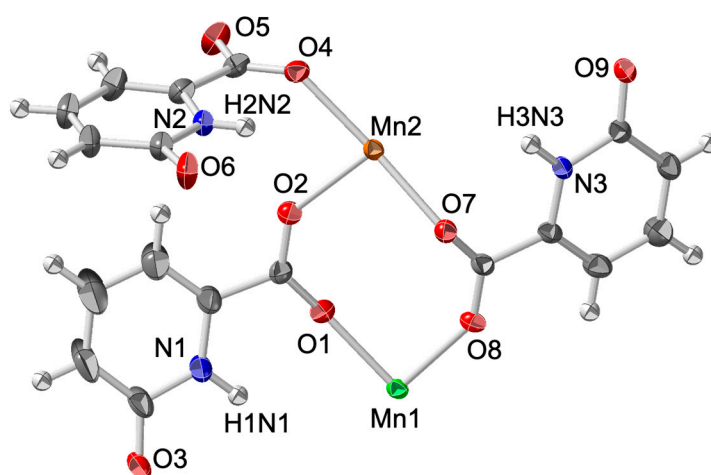


Figure 1. ORTEP diagram of the asymmetric unit with labelling scheme of compound **1**. Ellipsoids are drawn at 50% probability (except the H atoms).

Within the structure, all three HL^- ligands of the asymmetric unit act as non-chelating μ_3 -bridging ligands (Figure S3). Each ligand coordinates to two different Mn atoms using two carboxylate oxygen atoms in a *syn-anti* mode and coordinates to a third Mn atom through the deprotonated hydroxy group, giving rise to a 3D structure (see below). The

syn-anti carboxylate bridges connect two Mn centres to generate a chain with alternating Mn1-Mn2 (A-type) and Mn2-Mn2 (B-type) $[\text{Mn}_2(\text{RCOO})_2]$ units (Figure 2). These chains run parallel to the [101] direction. Along the chain, there are two A-type (Mn1-Mn2) and one B-type (Mn2-Mn2) units following the sequence -A-A-B- (Figure 2). These chains are further connected by four HL^- ligands through their keto groups in two other directions to form a 3D network (Figure 3). Interestingly, the pyridyl groups are protonated and do not coordinate with the metal centres, although they participate in $\text{N-H}\cdots\text{O}_{\text{hydroxy}}$ hydrogen bonding interactions within the structure and form two different $\text{R}_2^2(6)$ hydrogen-bonded supramolecular rings (Figure S4). All the hydrogen bond dimensions are given in Table S3.

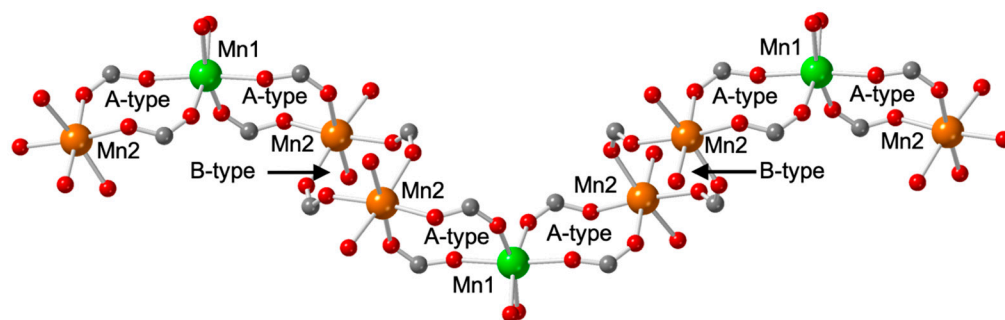


Figure 2. View of the $-\text{Mn}(\text{OC}(\text{R})\text{O})_2\text{-Mn}-$ chains formed by double *syn-anti* carboxylate bridges in **1** showing the A-type and B-type Mn dimers.

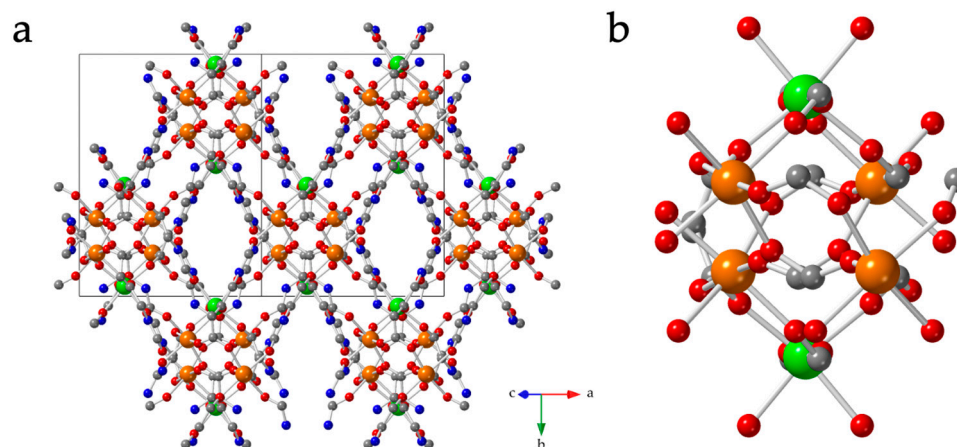


Figure 3. (a) Projection of the structure of compound **1** down the [101] direction (perpendicular to the chains). (b) View of one isolated chain along the same direction. Colour code: C = gray, O = red, N = blue, Mn1 = green, and Mn2 = orange.

3.3. Hirshfeld Surface Analysis

Hirshfeld surface (HS) analysis has been carried out to understand the intermolecular interactions present in compound **1**. The asymmetric unit has been used to calculate the Hirshfeld surface (such as d_{norm} , shape index, curvedness, and fragment patch) (Figure 4) and the subsequent Finger print plots (Figure 5 and Figure S5) to provide the qualitative and quantitative contribution of the noncovalent contacts present within the crystal system. The red, blue, and white colours used in d_{norm} indicate the interatomic distances closer, longer, or equal to van der Waals separations, respectively. On the other hand, valuable parameters of curvature, namely shape index and curvedness, have been included to offer further chemical insight into molecular shaping. A high curvedness is highlighted as dark blue edges in the shape index (Figure 4b) with ‘bumps and hollows’ depicted in blue and red, respectively, to indicate the flatness of the surface. The curvedness usually indicates large regions of green (relatively flat) separated by dark blue edges (large positive curvature) [48]. Figure 4 depicts the d_{norm} mapped surface showing light red spots near the

N-H where the deep spots are close to the O atoms, indicating the presence of O-H/H-O interactions. The 2D Finger Print plot (Figure 5) supports the N-H...O interactions between the protonated pyridyl groups and the oxygen atoms as the predominant interaction (17.10%). In addition, O...H/H...O hydrogen bonding interactions show a sharp spike at ($d_i = 1.10$ and $d_e = 0.75$ Å) and at ($d_i = 0.75$ Å and $d_e = 1.10$ Å). An additional contribution to the HS comes from the O-O (7.6%), C-C (4.1%), and N-H/H-N (1.9%) interactions.

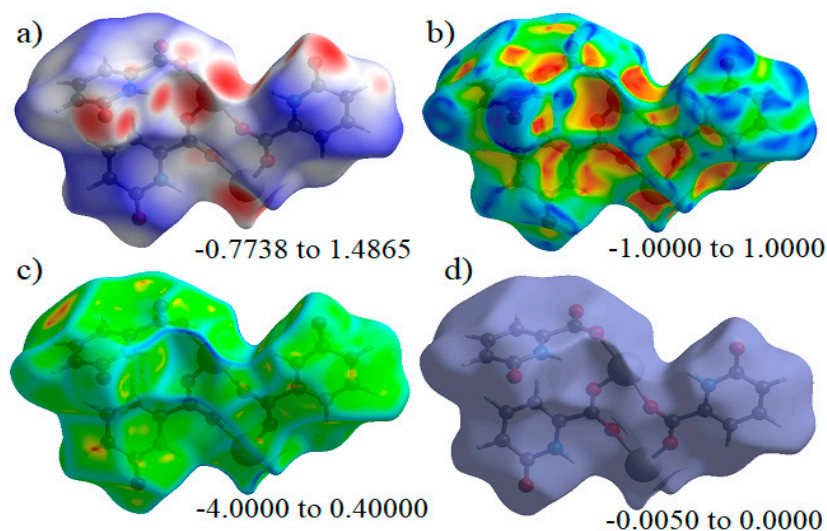


Figure 4. Hirshfeld surfaces mapped with (a) d_{norm} , (b) shape index, (c) curvedness, and (d) fragment patch for compound **1**.

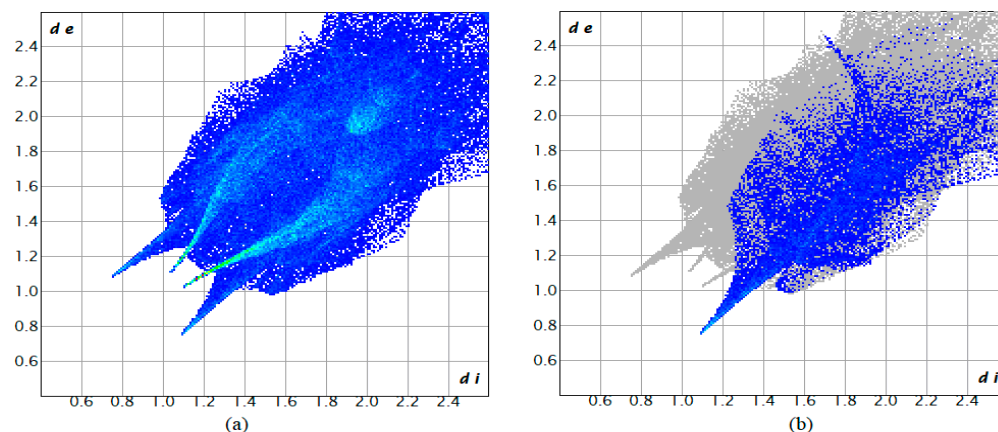


Figure 5. (a) Two-dimensional fingerprint plots for all contacts. (b) Two-dimensional fingerprint plot only for the O...H interactions.

3.4. Absorption and Emission Spectra of $[Mn_3(HL)_6]$ (**1**)

The solid-state absorption spectra of the colourless compound **1** show a peak at 319 nm with a shoulder at 328 nm and another small peak at 241 nm (Figure S6). The peak at 319 nm can be attributed to a ligand-to-metal charge transfer transition, whereas the peak at 241 nm can be assigned to the $n-\pi^*$ transition of the C=O bond that appears due to the *keto-enol* tautomerism. The emission spectra of compound **1** show one peak at 458 nm, which may be attributed to an intra-ligand $\pi-\pi^*$ transition (Figure S7).

3.5. Magnetic Properties

The product of the molar magnetic susceptibility times the temperature ($\chi_m T$) per Mn(II) ion for compound **1** shows at room temperature a value of ca. $4.4 \text{ cm}^3 \text{ K mol}^{-1}$, very close to the expected value for an isolated Mn(II) ion with a ground spin state $S = 5/2$

and a g value close to 2. When the sample is cooled, $\chi_m T$ slowly decreases, reaching a minimum value of $ca. 2.9 \text{ cm}^3 \text{ K mol}^{-1}$ at around 42 K, indicating the presence of a weak antiferromagnetic coupling (Figure 6). Below this temperature, $\chi_m T$ shows a sharp increase and reaches a value of $ca. 273 \text{ cm}^3 \text{ K mol}^{-1}$ at 10 K. This abrupt increase indicates the presence of a long-range magnetic ordering and suggests the presence of a spin-canting since the Mn–Mn coupling is antiferromagnetic. Below 10 K, $\chi_m T$ sharply decreases due to saturation effects in χ_m to reach a value of $ca. 90 \text{ cm}^3 \text{ K mol}^{-1}$ at 2 K. The thermal variation of χ_m shows a sharp divergence with a maximum slope at around 14 K, corresponding to the approximate temperature of the canted antiferromagnetic long-range order (Figure S8).

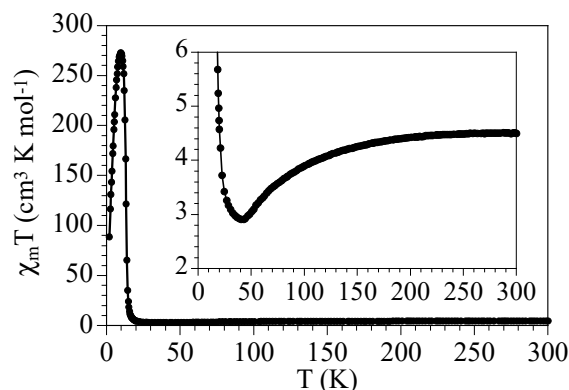


Figure 6. Thermal variation of $\chi_m T$ for compound **1**. Inset shows the high-temperature region.

Further confirmation of the canted ordering in **1** is provided by the isothermal magnetization at low temperatures that show an initial saturation value of $ca. 2 \mu_B$ (Figure S9) well below the expected one for an isolated Mn^{II} ion with $g \approx 2$ ($ca. 5 \mu_B$). Additionally, the isothermal magnetization shows hysteresis cycles of 40 mT at 2 K, 26 mT at 5 K, 7.5 mT at 10 K, and 2 mT at 12 K, indicating that the ordering temperature is above 12 K (Figure 7a). In fact, the thermal variation of the remnant magnetization obtained after cooling the sample under a magnetic field of 5 T shows a value of $ca. 1.05 \mu_B$ that vanishes above 14 K, confirming the presence of a canted antiferromagnetic order below $ca. 14 \text{ K}$ (Figure 7b).

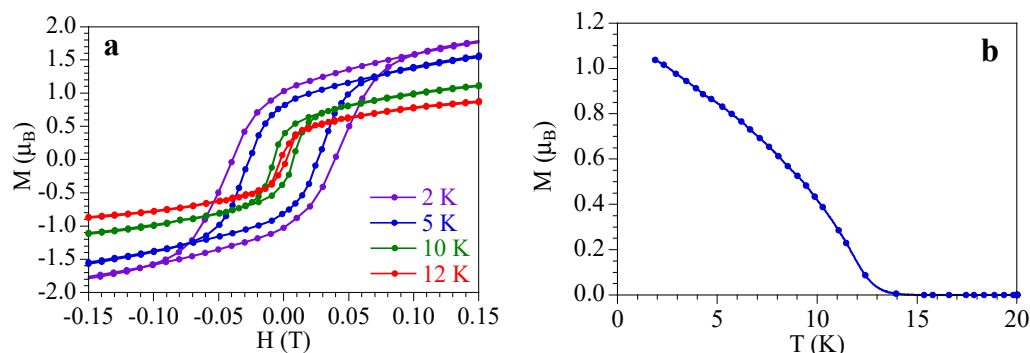


Figure 7. (a) Hysteresis cycles at different temperatures for compound **1**. (b) Thermal variation of the remnant magnetization of compound **1** after cooling the sample under 5 T.

To further confirm the presence of a long-range ordering, we have performed AC measurements of compound **1**. These measurements show a frequency-independent peak at around 13 K with an out-of-phase signal (χ''_m) that becomes non-zero below 14 K (Figure 8). This behaviour confirms the presence of a long-range order with an ordering temperature of 14 K.

Although not very common, the presence of a canted antiferromagnetic coupling between manganese ions through double and single *syn-anti* carboxylate bridges has already been reported in other manganese(II) [51] and manganese(III) [52,53] compounds

and has been attributed to the lack of a symmetry centre between the manganese ions, that favours the Dzyaloshinsky–Moriya (D-M) interaction along the *syn-anti* carboxylate bridge [54].

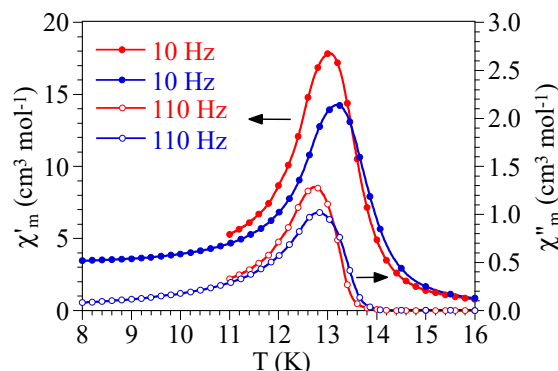


Figure 8. Thermal variation of the in-phase (χ'_{m} , left scale, filled circles) and out-of-phase (χ''_{m} , right scale, empty circles) signals of compound **1** at two different frequencies.

4. Conclusions

In summary, we have prepared and structurally characterized a new 3D manganese(II) compound formulated as $[\text{Mn}_3(\text{HL})_6]$ (**1**), with $\text{H}_2\text{L} = 6$ -hydroxypicolinic acid, that represents the first coordination polymer with this ligand and Mn(II) ions. The 3D structure of **1** can be described as zigzag Mn chains with double *syn-anti* carboxylate bridges that are further connected to four other chains by four HL^- ligands through their keto groups to generate a 3D coordination polymer. The 6-hydroxypicolinic acid-based ligand remains in its *keto* form in the structure with the proton located on the pyridyl N atom. Hirshfeld surface analysis indicates the presence of strong hydrogen bonding interactions between the protonated pyridyl N atoms and the oxygen atoms of the ligand within compound **1**. The DC and AC magnetic measurements show that compound **1** presents a weak antiferromagnetic Mn–Mn coupling through the double *syn-anti* carboxylate bridges but shows a long-range canted antiferromagnetic long-range order below 14 K with a coercive field of 40 mT at 2 K. This ligand demonstrates, thus, its capacity to construct 3D coordination polymers with interesting magnetic properties.

Supplementary Materials: The following supporting information can be downloaded at: <https://www.mdpi.com/article/10.3390/magnetochemistry9020055/s1>, Table S1: Structural data of all the reported structures with 6-hydroxypicolinic acid, Table S2: Coordination bond lengths (Å) and angles (°) in compound **1**, Table S3: Hydrogen bond dimensions for compound **1**; Figure S1: Simulated and experimental X-ray powder diffractograms for compound **1**, Figure S2: IR spectra of compound $[\text{Mn}(\text{HL})_2]$ (**1**), Figure S3: μ_3 -bridging mode of the ligand through carboxylate and hydroxy groups. Colour code: C = gray, O = red, N = blue, and Mn = purple), Figure S4: Hydrogen bonding interactions present in compound **1**. Colour code: C = black, O = red, N = blue, and Mn = green. Pink lines indicate the H-bonds, Figure S5: Two-dimensional fingerprint plots for (a) $\text{O}\cdots\text{H}$, (b) $\text{H}\cdots\text{O}$, (c) $\text{N}\cdots\text{H}$, (d) $\text{H}\cdots\text{N}$, (e) $\text{N}\cdots\text{O}$ and (f) $\text{O}\cdots\text{O}$ interactions, Figure S6: Solid-state absorption spectra of compound **1**, Figure S7: Solid-state emission spectra of compound **1**, Figure S8: Thermal variation of $\chi_{\text{m}}T$ for compound **1**. Inset shows the low-temperature region, Figure S9: Isothermal magnetization at different temperatures for compound **1**. CCDC number for compound **1** is 2232982. References [36,37,39,49,55–68] have been cited in Supplementary Materials.

Author Contributions: S.K.D., M.P., S.B. and R.S. have synthesized and characterized the material. K.G. has performed the Hirshfeld surface analysis. C.J.G.-G. have collected and analyzed the magnetic data. All the authors have written and revised the manuscript. All authors have read and agreed to the published version of the manuscript.

Funding: R.S. is beneficiary of the grant (Z21-070) for the requalification of the Spanish University system from the Ministry of Universities of the Government of Spain, modality “Maria Zambrano”, financed by the European Union. S.B. thankfully acknowledges DST Inspire Faculty Research Grant (DST/INSPIRE/04/2018/000329, Faculty Registration No.: IFA18-CH304). S.K.D. thanks DST Inspire Faculty Research Grant to S.K.D. for financial assistance. R.S. also acknowledges UGC for their STIDE GRANT to Kazi Nazrul University (Ref No: KNU/R/Letter/913/21). This research was funded by the Advanced Materials program and was supported by MCIN with funding from European Union NextGeneration EU (PRTR-C17.I1) and the Generalitat Valenciana (project MFA-2022-057). We also thank the Generalitat Valenciana (Prometeo/2019/076) and the project PID2021-125907NB-I00, financed by MCIN/AEI/10.13039/501100011033/FEDER, UE, for financial support.

Institutional Review Board Statement: Not applicable.

Informed Consent Statement: Not applicable.

Data Availability Statement: Data are available upon request to the corresponding authors.

Conflicts of Interest: The authors declare no conflict of interest.

References

1. Sakamaki, Y.; Tsuji, M.; Heidrick, Z.; Watson, O.; Durchman, J.; Salmon, C.; Burgin, S.R.; Beyzavi, H. Preparation and Applications of Metal–Organic Frameworks (MOFs): A Laboratory Activity and Demonstration for High School and/or Undergraduate Students. *J. Chem. Educ.* **2020**, *97*, 1109–1116. [[CrossRef](#)]
2. Furukawa, H.; Cordova, K.E.; O’Keeffe, M.; Yaghi, O.M. The Chemistry and Applications of Metal-Organic Frameworks. *Science* **2013**, *341*, 1230444. [[CrossRef](#)]
3. Kuppler, R.J.; Timmons, D.J.; Fang, Q.; Li, J.; Makal, T.A.; Young, M.D.; Yuan, D.; Zhao, D.; Zhuang, W.; Zhou, H. Potential applications of metal-organic frameworks. *Coord. Chem. Rev.* **2009**, *253*, 3042–3066. [[CrossRef](#)]
4. Chen, L.; Zhang, X.; Cheng, X.; Xie, Z.; Kuang, Q.; Zheng, L. The function of metal–organic frameworks in the application of MOF-based composites. *Nanoscale Adv.* **2020**, *2*, 2628. [[CrossRef](#)] [[PubMed](#)]
5. Russo, V.; Hmoudah, M.; Broccoli, F.; Iesce, M.R.; Jung, O.; Serio, M.D. Applications of Metal Organic Frameworks in Wastewater Treatment: A Review on Adsorption and Photodegradation. *Front. Chem. Eng.* **2020**, *2*, 581487. [[CrossRef](#)]
6. Thorarindottir, A.E.; Harris, T.D. Metal-Organic Framework Magnets. *Chem. Rev.* **2020**, *120*, 8716–8789. [[CrossRef](#)] [[PubMed](#)]
7. Yadav, S.; Dixit, R.; Sharma, S.; Dutta, S.; Solanki, K.; Sharma, R.K. Magnetic metal–organic framework composites: Structurally advanced catalytic materials for organic transformations. *Mater. Adv.* **2021**, *2*, 2153–2187. [[CrossRef](#)]
8. Gao, Y.; Liu, G.; Gao, M.; Huang, X.; Xu, D. Recent Advances and Applications of Magnetic Metal-Organic Frameworks in Adsorption and Enrichment Removal of Food and Environmental Pollutants. *Crit. Rev. Anal. Chem.* **2020**, *50*, 472–484. [[CrossRef](#)] [[PubMed](#)]
9. Kurmoo, M. Magnetic metal–organic frameworks. *Chem. Soc. Rev.* **2009**, *38*, 1353–1379. [[CrossRef](#)] [[PubMed](#)]
10. Coronado, E.; Espallargas, G.M. Dynamic magnetic MOFs. *Chem. Soc. Rev.* **2013**, *42*, 1525. [[CrossRef](#)]
11. Ricco, R.; Malfatti, L.; Takahashi, M.; Hill, A.J.; Falcaro, P. Applications of magnetic metal–organic framework composites. *J. Mater. Chem. A* **2013**, *1*, 13033. [[CrossRef](#)]
12. Ammari, Y.; Baaalla, N.; Hlil, E.K.; Abid, S. Structure, optical and magnetic properties of a novel homometallic coordination polymers: Experimental and computational studies. *Nat. Sci. Rep.* **2020**, *10*, 1316. [[CrossRef](#)] [[PubMed](#)]
13. Wang, H.; Wu, Y.; Leong, C.F.; D’Alessandro, D.M.; Zuo, J. Crystal Structures, Magnetic Properties, and Electrochemical Properties of Coordination Polymers Based on the Tetra(4-pyridyl)-tetrathiafulvalene Ligand. *Inorg. Chem.* **2015**, *54*, 10766–10775. [[CrossRef](#)]
14. Shao, D.; Moorthy, S.; Yang, X.; Yang, J.; Shi, L.; Singh, S.K.; Tian, Z. Tuning the structure and magnetic properties via distinct pyridine derivatives in cobalt(II) coordination polymers. *Dalton Trans.* **2022**, *51*, 695. [[CrossRef](#)] [[PubMed](#)]
15. Zhang, Y.; Gao, L.; Zhou, W.; Wei, X.; Hu, T. Synthesis and magnetic properties of two Mn based coordination polymers constructed by a mixed-ligand strategy. *CrystEngComm* **2020**, *22*, 7123. [[CrossRef](#)]
16. Pajuelo-Corral, O.; García, J.A.; Castillo, O.; Luque, A.; Rodríguez-Diéguez, A.; Cepeda, J. Single-Ion Magnet and Photoluminescence Properties of Lanthanide(III) Coordination Polymers Based on Pyrimidine-4,6-Dicarboxylate. *Magnetochemistry* **2021**, *7*, 8. [[CrossRef](#)]
17. Zhou, Y.; Hong, M.; Wu, X. Lanthanide–transition metal coordination polymers based on multiple N- and O-donor ligands. *Chem. Commun.* **2006**, *2*, 135–143. [[CrossRef](#)] [[PubMed](#)]
18. Feng, X.; Liu, L.; Wang, L.; Song, H.; Qiang, Z.; Wu, S.X.; Ng, S. Lanthanide coordination polymers based on multi-donor ligand containing pyridine and phthalate moieties: Structures, luminescence and magnetic properties. *J. Solid State Chem.* **2013**, *206*, 277–285. [[CrossRef](#)]
19. Robin, A.Y.; Fromm, K.M. Coordination polymer networks with O- and N-donors: What they are, why and how they are made. *Coord. Chem. Rev.* **2006**, *250*, 2127–2157. [[CrossRef](#)]
20. Galán-Mascarós, J.R.; Dunbar, K.R. A Self-Assembled 2D Molecule-Based Magnet: The Honeycomb Layered Material {Co₃Cl₄(H₂O)₂[Co(Hbbiz)₃]₂}. *Angew. Chem. Int. Ed.* **2003**, *42*, 2289. [[CrossRef](#)]

21. Maspoch, D.; Ruiz-Molina, D.; Veciana, J. Magnetic nanoporous coordination polymers. *J. Mater. Chem.* **2004**, *14*, 2713. [[CrossRef](#)]
22. Poulsen, R.D.; Bentien, A.; Chevalier, M.; Iversen, B.B. Synthesis, Physical Properties, Multitemperature Crystal Structure, and 20 K Synchrotron X-ray Charge Density of a Magnetic Metal Organic Framework Structure, $Mn_3(C_8O_4H_4)_3(C_5H_{11}ON)_2$. *J. Am. Chem. Soc.* **2005**, *127*, 9156. [[CrossRef](#)] [[PubMed](#)]
23. Miyasaka, H.; Clérac, R.; Mizushima, K.; Sugiura, K.I.; Yamashita, M.; Wernsdorfer, W.; Coulon, C. $[Mn_2(\text{saltmen})_2Ni(\text{pao})_2(L)_2](A)_2$ with L = Pyridine, 4-Picoline, 4-*tert*-Butylpyridine, *N*-Methylimidazole and A = ClO_4^- , BF_4^- , PF_6^- , ReO_4^- : A Family of Single-Chain Magnets. *Inorg. Chem.* **2003**, *42*, 8203–8213. [[CrossRef](#)] [[PubMed](#)]
24. Clérac, R.; Miyasaka, H.; Yamashita, M.; Coulon, C. Evidence for Single-Chain Magnet Behavior in a Mn^{III} – Ni^{II} Chain Designed with High Spin Magnetic Units: A Route to High Temperature Metastable Magnets. *J. Am. Chem. Soc.* **2002**, *124*, 12837–12844. [[CrossRef](#)]
25. Kimura, S.; Matsuoka, R.; Kimura, S.; Nishihara, H.; Kusamoto, T. Radical-Based Coordination Polymers as a Platform for Magnetoluminescence. *J. Am. Chem. Soc.* **2021**, *143*, 5610–5615. [[CrossRef](#)]
26. Yong, G.; Qiao, S.; Wang, Z. A One-Dimensional Coordination Polymer Based on Novel Radical Anion Ligand Generated In Situ: Notable Magnetic and Luminescence Properties. *Cryst. Growth Des.* **2008**, *8*, 1465–1467. [[CrossRef](#)]
27. Benmansour, S.; Abherve, A.; Gómez-Claramunt, P.; Vallés-García, C.; Gómez-García, C.J. Nanosheets of Two-Dimensional Magnetic and Conducting Fe(II)/Fe(III) Mixed-Valence Metal–Organic Frameworks. *ACS Appl. Mater. Interfaces* **2017**, *9*, 26210–26218. [[CrossRef](#)]
28. Aulakh, D.; Liu, L.; Varghese, J.R.; Xie, H.; Islamoglu, T.; Duell, K.; Kung, C.; Hsiung, C.; Zhang, Y.; Drout, R.J.; et al. Direct Imaging of Isolated Single-Molecule Magnets in Metal–Organic Frameworks. *J. Am. Chem. Soc.* **2019**, *141*, 2997–3005. [[CrossRef](#)]
29. Palacios-Corella, M.; García-López, V.; Sánchez-Sánchez, C.; Clemente-Juan, J.M.; Clemente-León, M.; Coronado, E. Insertion of single-ion magnets based on mononuclear Co(II) complexes into ferromagnetic oxalate-based networks. *Dalton Trans.* **2021**, *50*, 5931. [[CrossRef](#)]
30. Kusumoto, S.; Umeno, H.; Kim, Y.; Sekine, Y.; Nakamura, M.; Hayami, S. Structural and Magnetic Characterization of Homo- and Heterometallic Trinuclear Ni(II) and Cu(II) Clusters with N_2O_6 Acyclic Polydentate Ligand. *Chem. Lett.* **2021**, *50*, 1945–1948. [[CrossRef](#)]
31. Andrews, P.C.; Deacon, G.B.; Frank, R.; Fraser, B.H.; Junk, P.C.; MacLellan, J.G.; Massi, M.; Moubaraki, B.; Murray, K.S.; Silberstein, M. Formation of Ho(III) Trinuclear Clusters and Gd(III) Monodimensional Polymers Induced by ortho and para Regioisomers of Pyridyl-Functionalised β -Diketones: Synthesis, Structure, and Magnetic Properties. *Eur. J. Inorg. Chem.* **2009**, *2009*, 744–751. [[CrossRef](#)]
32. Gao, E.; Liu, N.; Cheng, A.; Gao, S. Novel frustrated magnetic lattice based on triangular $[Mn_3(\mu_3-F)]$ clusters with tetrazole ligands. *Chem. Commun.* **2007**, *24*, 2470–2472. [[CrossRef](#)] [[PubMed](#)]
33. Sawada, K.; Ohashi, Y. 2-Oxo-1,2-dihydropyridine-6-carboxylic Acid. *Acta Cryst.* **1998**, *C54*, 1491–1493. [[CrossRef](#)]
34. Kazemi, S.H.; Eshtiagh-Hosseini, H.; Izadyar, M.; Mirzaei, M. Computational Study of the Intramolecular Proton Transfer between 6-Hydroxypicolinic Acid Tautomeric Forms and Intermolecular Hydrogen Bonding in their Dimers. *Phys. Chem. Res.* **2013**, *1*, 117–125.
35. Liu, C.; Song, Y. An Uneven Chain-like Ferromagnetic Copper(II) Coordination Polymer Displaying Metamagnetic Behavior and Long-Range Magnetic Ordering. *Magnetochemistry* **2022**, *8*, 2. [[CrossRef](#)]
36. Sun, C.; Zheng, X.; Li, W.; Wang, M.; Fang, C. Assembly of Supramolecular Networks with the Inclusion of Water Chains, Cyclic Hepta and Octa Water Clusters. *Z. Anorg. Allg. Chem.* **2008**, *634*, 2663–2669. [[CrossRef](#)]
37. Bian, G.Q.; Kuroda-Sowa, T.; Konaka, H.; Maekawa, M.; Munakata, M. Bis(μ -6-hydroxypicolinato)- μ -oxobis[dipyridinemanganese (III)] monohydrate. *Acta Crystallogr. Sect. C* **2004**, *60*, m338–m340. [[CrossRef](#)]
38. Sun, C.; Zheng, X.; Jin, L.Z. Syntheses and Structures of the First Examples of Lanthanide Complexes with 6-Hydroxypicolinic Acid. *Z. Anorg. Allg. Chem.* **2004**, *630*, 1342–1347. [[CrossRef](#)]
39. Kukovec, B.; Vaz, P.D.; Calhorda, M.J.; Popovic, Z. Disappearing and Concomitant Polymorphism of Nickel(II) Complexes with 6-Hydroxypicolinic Acid. Structural and Density Functional Theory Studies. *Cryst. Growth Des.* **2010**, *10*, 3685–3693. [[CrossRef](#)]
40. Bruker, APEX2, SAINT and SADABS, BRUKER AXS, Inc.: Madison, WI, USA, 2008.
41. Sheldrick, G.M. A short history of SHELX. *Acta Cryst.* **2008**, *A64*, 112. [[CrossRef](#)]
42. Farrugia, L.J. WinGX and ORTEP for Windows, an update. *J. Appl. Crystallogr.* **2012**, *45*, 849. [[CrossRef](#)]
43. Sheldrick, G.M. Crystal structure refinement with SHELX. *Acta Cryst.* **2015**, *C71*, 3.
44. Spek, A.L. Structure validation in chemical crystallography. *Acta Cryst.* **2009**, *D65*, 148. [[CrossRef](#)] [[PubMed](#)]
45. Farrugia, L.J. ORTEP-3 for Windows—A version of ORTEP-III with a Graphical User Interface (GUI). *J. Appl. Crystallogr.* **1997**, *30*, 565. [[CrossRef](#)]
46. Bain, G.A.; Berry, J.F. Diamagnetic corrections and Pascal’s constants. *J. Chem. Educ.* **2008**, *85*, 532–536. [[CrossRef](#)]
47. McKinnon, J.J.; Jayatilaka, D.; Spackman, M.A. Towards quantitative analysis of intermolecular interactions with Hirshfeld surfaces. *Chem. Commun.* **2007**, *37*, 3814–3816. [[CrossRef](#)]
48. Spackman, M.A.; McKinnon, J.J. Fingerprinting intermolecular interactions in molecular crystals. *CrystEngComm* **2002**, *4*, 378–392. [[CrossRef](#)]
49. Kukovec, B.; Popovića, Z.; Pavlović, G.; Linarić, M.R. Synthesis and structure of cobalt(II) complexes with hydroxyl derivatives of pyridinecarboxylic acids: Conformation analysis of ligands in the solid state. *J. Mol. Struct.* **2008**, *882*, 47–55. [[CrossRef](#)]

50. Blatov, V.A.; Shevchenko, A.P.; Proserpio, D.M. Applied Topological Analysis of Crystal Structures with the Program Package ToposPro. *Cryst. Growth Des.* **2014**, *14*, 3576–3586. [[CrossRef](#)]
51. Wang, X.; Wei, H.; Wang, Z.; Chen, Z.; Gao, S. Formate—The Analogue of Azide: Structural and Magnetic Properties of $M(\text{HCOO})_2(4,4'\text{-Bpy})\cdot n\text{H}_2\text{O}$ ($M = \text{Mn, Co, Ni}$; $n = 0, 5$). *Inorg. Chem.* **2005**, *44*, 572–583. [[CrossRef](#)]
52. Kar, P.; Guha, P.M.; Drew, M.G.B.; Ishida, T.; Ghosh, A. Spin-Canted Antiferromagnetic Phase Transitions in Alternating Phenoxo- and Carboxylato-Bridged Mn(III)-Salen Complexes. *Eur. J. Inorg. Chem.* **2011**, *2011*, 2075–2085. [[CrossRef](#)]
53. Mossin, S.; Weihe, H.; Osholm Sørensen, H.; Lima, N.; Sessoli, R. Rationalisation of Weak Ferromagnetism in Manganese(III) Chains: The Relation between Structure and Ordering Phenomena. *Dalton Trans.* **2004**, *4*, 632–639. [[CrossRef](#)] [[PubMed](#)]
54. Kahn, O. *Molecular Magnetism*; VCH Publishers: New York, NY, USA, 1993.
55. Kang, S.K.; Shim, Y.S. Poly[(m6-6-Oxidopyridinium-2-Carboxylato)Caesium]. *Acta Cryst. E* **2011**, *67*, m1237. [[CrossRef](#)]
56. Małecki, J.G.; Krompiec, S.; Maroń, A.; Penkala, M. Synthesis, Molecular, Spectroscopic and Catalytic Characterization of Ruthenium(II) Complexes with Pyridine-2-Carboxylic Acid Derivatives Ligands. *Polyhedron* **2012**, *48*, 21–30. [[CrossRef](#)]
57. Kukovec, B.-M.; Popovic, Z.; Pavlovic, G. Copper(II) Complexes with 3- and 6-hydroxypicolinic Acid. Preparation, Structural, Spectroscopic and Thermal Study. *Acta Chim. Slov.* **2008**, *55*, 779–787.
58. Kukovec, B.M.; Kaksa, M.; Popovic, Z. Synthesis and Characterization of a Copper(II) Complex with 6-Hydroxypicolinic Acid and 3-Picoline Croatica. *Chem. Acta* **2012**, *85*, 479–483.
59. Sengül, A.; Büyükgüngör, O. Trans-Di-Aqua-Bis(6-Hydroxy-Picolinato-k2-N,O2)Copper(II). *Acta Cryst. E* **2005**, *61*, m119–m121.
60. You-Zhu Yu, Song-Yang Chang, Xi Han, Guang-Xin Chen, Ya-Wei Xuan, Xian-Li Wu, Fang Wang, Hydrothermal Syntheses, Crystal Structures and Luminescence Properties of Cu(II) and Cd(II) Complexes Assembled by 6-Hydroxypicolinic Acid and 1,10-Phenanthroline. *Jiegou Huaxue* **2019**, *38*, 651–659.
61. Sun, C.; Zhou, J.; Li, W.; Jin, L. Supramolecular Structures from Mononuclear, Binuclear and 2D Net of Copper(II) Complexes with 6-Hydroxypicolinic Acid. *Z. Anorg. Allg. Chem.* **2008**, *634*, 549–554. [[CrossRef](#)]
62. Su, W.; Guo, Y.; Yu, Y.; Wang, Y. Synthesis, Structure and Magnetic Property of a Linear Trinuclear Dy(III) Single Molecular Magnet. *Inorg. Chem. Commun.* **2020**, *120*, 108161. [[CrossRef](#)]
63. Nakasone, T.; Nishioka, T.; Asato, E.; Kinoshita, I.; Takara, S. Synthesis and Structural Characterization of Novel Ruthenium(II) Complexes Bearing Hydroxypicolinato Ligands. *Polyhedron* **2012**, *45*, 152–157. [[CrossRef](#)]
64. Casas, J.S.; Castellano, E.E.; Ellena, J.; García-Tasende, M.S.; Sánchez, A.; Sordo, J.; Toma, M. Dimethylthallium(III) Complexes with Picolinic Acid and its Hydroxyl Derivatives. *Polyhedron* **2008**, *27*, 1296–1302. [[CrossRef](#)]
65. Chattopadhyay, S.; Fanwick, P.E.; Walton, R.A. Reactions of the Triply-Bonded Complex $\text{cis-Re}_2(\mu\text{-O}_2\text{CCH}_3)_2\text{Cl}_2(\mu\text{-Dppm})_2$ with Pyridine Carboxylic Acids. the Isolation and Structural Characterization of a Third Structural Isomer of $\text{Re}_2(\text{Dipic})\text{Cl}_2(\mu\text{-Dppm})_2$ (Dipic = Pyridine-2,6-Dicarboxylate). *Dalton Trans.* **2003**, *18*, 3617–3621. [[CrossRef](#)]
66. Mukiza, J.; Hosten, E.C.; Gerber, T.I.A. Rhenium(III), (IV) and (V) Complexes with 6-Hydroxypicolinic Acid. *Polyhedron* **2016**, *110*, 106–113. [[CrossRef](#)]
67. Nakama, Y.; Nishioka, T.; Nakasone, T.; Asato, E.; Kinoshita, I.; Takara, S. Synthesis And Crystal Structure of $[\text{RuCl}(\text{6-hydroxypicolinato})(2,2';6',2''\text{-terpyridine})]\cdot(\text{N,N-dimethylformamide})$. *X-ray Struct. Anal. Online* **2010**, *26*, 33–34. [[CrossRef](#)]
68. Sun, C.; Jin, L. Supramolecular Architectures from the Self-Assembly of Lanthanide Ions with 6-Hydroxypicolinic Acid and 1,10-Phenanthroline. *J. Mol. Struct.* **2005**, *741*, 241–247. [[CrossRef](#)]

Disclaimer/Publisher’s Note: The statements, opinions and data contained in all publications are solely those of the individual author(s) and contributor(s) and not of MDPI and/or the editor(s). MDPI and/or the editor(s) disclaim responsibility for any injury to people or property resulting from any ideas, methods, instructions or products referred to in the content.